IEEE Access
Multidisciplinary | Rapid Review | Open Access Journal

Received November 7, 2019, accepted November 26, 2019, date of publication November 29, 2019,
date of current version December 13, 2019.

Digital Object Identifier 10.1109/ACCESS.2019.2956743

Design of Robust Observers for Active Roll Control

MANBOK PARK[1] AND SEONGJIN YIM[2], (Member, IEEE)
[1]Korea National University of Transportation, Chungju 27469, South Korea
[2]Research Center for Electrical and Information Technology, Seoul National University of Science and Technology, Seoul 01811, South Korea

Corresponding author: Seongjin Yim (acebtif@seoultech.ac.kr)

This work was supported by the National Research Foundation of South Korea (NRF) Grant funded by the Korean Government through the Ministry of Education under Grant 2019R1A6A1A03032119.

ABSTRACT This paper presents robust observers for active roll control. Generally, active roll control adopts feedback control structure with roll angle and roll rate signals which should be measured with a sensor. For active roll control, it is necessary to estimate the roll angle with roll rate measurement using an observer because the roll angle is difficult to measure, compared to the roll rate. However, an observer designed with fixed parameters can give poor estimation performance since there are large uncertainty in parameters of real vehicles. A robust observer is designed to cope with the parameter uncertainty. In this paper, a dual Kalman filter and Kalman filter with constant velocity model are adopted as a robust observer. The performance of the proposed algorithm has been investigated via computer simulations and vehicle tests.

INDEX TERMS Active roll control, parameter uncertainty, robust observer, dual Kalman filter, Kalman filter with constant velocity model.

NOMENCLATURE

g	gravitational acceleration (9.81 m/s^2)
h_s	height of C.G. from a roll center (m)
I_{xx}	roll moment of inertia about roll axis (kg·m^2)
m_s	sprung mass of a vehicle (kg)
T_s	sampling period (sec)
ϕ	roll angle (rad)
$\dot{\phi}$	roll rate (rad/s)
$\mathbf{x}_s$	state vector of the state estimators (dual KF, KFCVM)
$\mathbf{x}_p$	state vector of the parameter estimator (dual KF)

I. INTRODUCTION

Two major factors generating the vehicle roll motion are the lateral acceleration and the road profile. Generally, road profile and lateral acceleration, as a disturbance, can generate the vehicle roll motion with the frequency below and over 1Hz, respectively. Active roll control (ARC) is developed to control the vehicle roll motion against these disturbances. There are two objectives in ARC. The first is to reduce the roll angle and the roll rate for ride comfort, and the second is to reduce the suspension stroke and tire deflection to prevent vehicle rollover. These objectives can be represented as a disturbance attenuation problem [1]. Active suspension, semi-active suspension and active anti-roll bar (AARB) have been used as an actuator for ARC [2]. An active suspension can control the vertical, roll and pitch motion of sprung mas of a vehicle. On the other hand, an AARB can control only the roll motion of a vehicle. In this paper, an AARB is adopted as an actuator for ARC.

There have been several researches for ARC [3]–[8]. These include the discrete-time LQR [3], [4], the PD control [5], LQG-LTR control [6], H_∞ control [3], [4], [7], [9], and sliding mode control [3], [4], [8], [10], etc. Most of active roll controllers in these researches have adopted feedback control structure with measured signals of roll angle and roll rate. In real vehicles, it is too difficult to measure the roll angle with a sensor, and a roll angle sensor is so expensive. Compared to the roll angle, it is relatively easy to measure the roll rate with commercial gyro sensors. Up to date, several roll rate sensors have been commercialized at a reasonable price [11]–[13]. For the reason, a Kalman filter (KF), as a state observer, has been adopted to estimate the roll angle using measured roll rate signal for feedback control [4], [6], [11]. This is called an observer-based controller or output feedback controller. The schematic diagram of observer-based active roll controller is

The associate editor coordinating the review of this manuscript and approving it for publication was Shihong Ding.

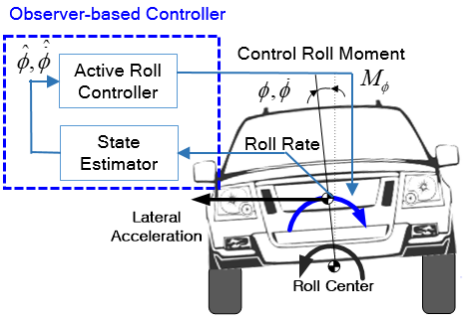

FIGURE 1. Schematic diagrams of observer-based active roll controller with state estimator.

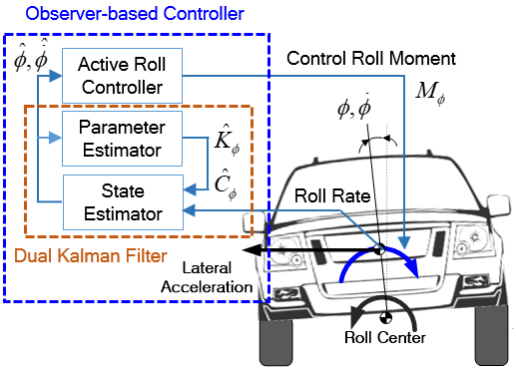

FIGURE 2. Schematic diagram of observer-based active roll controller with state and parameter estimators.

shown in Fig. 1. In this paper, the roll angle is estimated using a KF with roll rate measurement.

In real vehicles, vehicle parameters are uncertain and vary over time. In view of ARC, there are parameter uncertainties in the roll damping, the roll stiffness, the moment of inertia and the height of C.G. Moreover, there are nonlinearities in roll dynamics of vehicles. To estimate states under parameter uncertainties and nonlinearities, it is necessary to design an observer robust against the parameter uncertainty and nonlinearity. For the purpose, there have been two schemes: robust and parameter estimation.

In case of robust estimation scheme, an observer is designed with robust control methodology with norm-bounded uncertainty model so as to be robust against the parameter variation [9], [14]. Another method for robust estimation scheme is to include the nonlinear and time-varying effects in the dynamic model. In the previous work, the vehicle speed was considered as a time-varying term for ARC [7]. Recently, a nonlinear observer with neural networks and H_∞ filtering have been proposed for roll angle estimation [15], [16]. To incorporate the nonlinear effect of vehicle dynamics, Takagi-Sugeno(T-S) fuzzy model was adopted to design an observer when estimating the roll angle and the roll rate [17]–[19]. This scheme has been known to be effective in coping with parameter variations. However, the design procedure is complicated.

In case of parameter estimation scheme, time-varying or uncertain parameters are estimated by parameter adaptation methods such as least-mean-square (LMS) and recursive-least-square (RLS) algorithms [20]–[23]. For roll angle estimation, RLS was used to estimate the height of center of gravity [20]. Roll dynamics was identified with RLS for sliding mode state observer [21]. Compared to robust estimation schemes, this is simple to design and easy to implement. So, this paper adopts parameter estimation scheme, especially, RLS. RLS can be represented with KF. With the idea, a dual extended KF have been adopted for simultaneous estimation of state and parameter in vehicle control [24], [25]. Following the idea of parameter estimation with KF, the dual KF is adopted as a robust observer when estimating states and parameters simultaneously for ARC. The schematic diagram of observer-based active roll controller with state and parameter estimators is shown in Fig. 2.

Most of Kalman filters that have been adopted as a state estimator use a system model. This is called a model-based observer. In case of a model-based observer, there are more likely to be give poor estimation performance if there are uncertainties in model parameters. So, an observer can be robust against parameter uncertainty if it is independent of system parameters. Typical example of the parameter independent KF is a KF with constant velocity model (KFCVM) [26]–[28]. KFCVM can be used as a state estimator and noise filter. If a roll rate signal is fed into KFCVM, the filtered roll rate and the estimated roll angle are obtained from it. In this paper, KFCVM is adopted as a robust observer.

In this paper, the observer-based controller is designed. Three feedback controllers, i.e., discrete-time LQR, H_∞ and sliding mode controller(SMC), are adopted as an active roll controller. Second, two KFs, i.e., dual KF and KFCVM are designed as a robust observer. The contribution of this paper is to validate the robustness of three KFs, i.e., KF with fixed parameters (KFFP), dual KF and KFCVM, against parameter uncertainties and nonlinearities through simulation on a vehicle simulation software, CarSim, and experiments on a real vehicle. For the purpose, the simulation and experiment are done on observer-based controllers, which combine three active roll controllers and three KFs with a large number of sets of model parameters randomly generated from given ranges.

This paper consists of the following parts. Three active roll controllers are designed with a 1-DOF roll model in section 2. In section 3, discrete-time Kalman filter, dual KF, and KFCVM are designed. In section 4, the designed robust observers are validated via simulation on CarSim and by experiment on a test vehicle. Finally, conclusions are provided in Section 5.

II. DESIGN OF ACTIVE ROLL CONTROLLERS

A. VEHICLE MODEL AND DISCRETE-TIME STATE-SPACE EQUATION

In this paper, a 1-DOF linear model is used in designing active roll controllers and KFs [3], [10]. Fig. 3 shows the

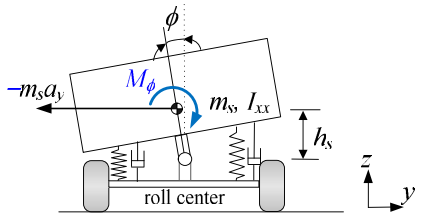

FIGURE 3. 1-DOF roll model.

1-DOF roll model. From the model, the equation of the motion is derived as (1). In the model, the control input and the disturbance are the control roll moment M_ϕ and the lateral acceleration a_y, respectively. C_ϕ and K_ϕ are the roll damping coefficient and the roll stiffness, respectively. Using the state vector (2), the continuous-time state-space equation is derived as (3). With the sampling time of T_s, the discrete-time state-space equation is obtained as (4) by discretizing (3) [3], [4].

$$I_{xx}\ddot{\phi}(t) + C_\phi\dot{\phi}(t) + K_\phi\phi(t) = M_\phi(t) + m_s h_s a_y(t) \quad (1)$$

$$\mathbf{x}(t) \equiv \left[\phi(t)\ \dot{\phi}(t)\right]^T \quad (2)$$

$$\dot{\mathbf{x}}(t) = \mathbf{A}\mathbf{x}(t) + \mathbf{B}_1 a_y(t) + \mathbf{B}_2 M_\phi(t) = \begin{bmatrix} 0 & 1 \\ -\frac{K_\phi}{I_{xx}} & -\frac{C_\phi}{I_{xx}} \end{bmatrix}\mathbf{x}(t) + \begin{bmatrix} 0 \\ \frac{m_s h_s}{I_{xx}} \end{bmatrix} a_y(t) + \begin{bmatrix} 0 \\ \frac{1}{I_{xx}} \end{bmatrix} M_\phi(t) \quad (3)$$

$$\mathbf{x}(k+1) = \mathbf{\Phi}\mathbf{x}(k) + \mathbf{\Gamma}a_y(k) + \mathbf{\Omega}M_\phi(k) \quad (4)$$

B. CONTROLLER DESIGN FOR ARC

Based on the linear model (4), three active roll controllers–discrete-time LQR, H_∞ and sliding mode controllers–were designed following the previous work [3], [4]. In the observer-based active roll controller, these controllers are used for ARC, as shown in Fig. 2. Generally, an active roll controller consists of two parts: feedback and feedforward ones. In this paper, only feedback is adopted for ARC. The stability of these controllers is guaranteed through design methodology of LQR, H_∞ and sliding mode controllers, as given in the previous work [3]. The feedback controller uses the state (2). So, the roll angle and the roll rate should be measured. However, it is hard to measure the roll angle. So, a state observer or Kalman filter is designed to estimate the roll angle with roll rate measurement.

III. DESIGN OF ROBUST OBSERVERS

A. KALMAN FILTER

The system and output equations of a discrete-time state-space model driven by white noises are given in (5). In (5), $\mathbf{M}(k)$ and $\mathbf{N}(k)$ are the covariance matrices of the system and sensor noises, $\mu(k)$ and $\eta(k)$, respectively. The equations of Kalman filter are given in (6) and (7), which represent the time- and measurement-updates, respectively [29]. For Kalman filter design, the system matrices $\mathbf{F}$, $\mathbf{G}$ and $\mathbf{H}$, and the covariance matrices of system and measurement noises, $\mathbf{M}$ and $\mathbf{N}$, should be determined.

$$\begin{cases} \mathbf{x}(k+1) = \mathbf{F}\mathbf{x}(k) + \mathbf{G}\mathbf{w}(k) + \mathbf{H}\mathbf{u}(k) + \boldsymbol{\mu}(k) \\ \mathbf{y}(k) = \mathbf{C}\mathbf{x}(k) + \boldsymbol{\eta}(k) \end{cases} \quad (5)$$

$$\mathbf{M}(k) = \mathbb{E}\left\{\boldsymbol{\mu}(k)\boldsymbol{\mu}^T(k)\right\},\ \mathbf{N}(k) = \mathbb{E}\left\{\boldsymbol{\eta}(k)\boldsymbol{\eta}^T(k)\right\}$$

$$\begin{cases} \hat{\mathbf{x}}_-(k) = \mathbf{F}\hat{\mathbf{x}}(k-1) + \mathbf{G}\mathbf{w}(k-1) + \mathbf{H}\mathbf{u}(k-1) \\ \bar{\mathbf{P}}(k) = \mathbf{M}(k) + \mathbf{F}\mathbf{P}(k-1)\mathbf{F}^T \end{cases} \quad (6)$$

$$\begin{cases} \mathbf{K}_e = \bar{\mathbf{P}}(k)\mathbf{C}^T\left[\mathbf{N}(k) + \mathbf{C}\bar{\mathbf{P}}(k)\mathbf{C}^T\right] \\ \hat{\mathbf{x}}(k) = \hat{\mathbf{x}}_-(k) + \mathbf{K}_e\left[\mathbf{y}(k) - \mathbf{C}\hat{\mathbf{x}}_-(k)\right] \\ \mathbf{P}(k) = (\mathbf{I} - \mathbf{K}_e\mathbf{C})\bar{\mathbf{P}}(k) \end{cases} \quad (7)$$

B. KALMAN FILTER FOR STATE ESTIMATION

For state estimation with KF, the matrices in (5) should be set as given in (9) with the state definition (8) from the discrete-time state-space model (4). The sensor output used for state estimation is the roll rate. So, the output matrix $\mathbf{C}$ is set as (9).

$$\mathbf{x}_s = \left[\phi\ \dot{\phi}\right]^T \quad (8)$$

$$\mathbf{F} = \mathbf{\Phi},\quad \mathbf{G} = \mathbf{\Gamma},\quad \mathbf{H} = \mathbf{\Omega},\quad \mathbf{C} = \left[0\ 1\right] \quad (9)$$

The continuous-time observability of [$\mathbf{A}$,$\mathbf{C}$] from (3) and (9) can be checked with the rank of observability matrix. With [$\mathbf{A}$,$\mathbf{C}$], the observability matrix $\mathbf{M}_O$ is calculated as (10). The necessary condition for observability is that the rank of $\mathbf{M}_O$ should be 2. This is always guaranteed if K_ϕ and C_ϕ are positive, as shown in (10). Therefore, the observer-based control system is globally stable with LQR, H_∞, sliding mode controllers and a KF in terms of the separation principle.

$$\mathbf{M}_O = \left[\mathbf{C}^T\ \mathbf{A}^T\mathbf{C}^T\right] = \frac{1}{I_{xx}}\begin{bmatrix} 0 & -K_\phi \\ I_{xx} & -C_\phi \end{bmatrix} \quad (10)$$

C. KALMAN FILTER FOR PARAMETER ESTIMATION

Besides KF for state estimation, it can be used for parameter estimation. In RLS, the definitions on output and error are given from (11) and (12). In (11), $\phi(k)$ and $\theta(k)$ are the vectors of measurements and the unknown parameters to be estimated at time instant k, respectively. RLS as a parameter estimator has been combined with KF as a state estimator [20]–[23]. RLS can be represented by KF [24], [25]. Following the previous works, a KF, which is equivalent to RLS, is used as a parameter estimator in this paper.

$$y(k) = \phi^T(k)\theta(k) + e(k) \quad (11)$$

$$e(k+1) = y(k) - \phi^T(k+1)\hat{\theta}(k) \quad (12)$$

The discrete-time state-space model equations driven by white noise processes $\mu_2(k)$ and $\eta_2(k)$ is given in (13). The output equation (11) can be converted into (13). In (13), $\mathbf{x}_p(k)$ the vector of parameters to be estimated, and $\phi^T(k)$ is the output vector as defined from (14) to (17). As shown from (14) to (17), the parameters to be estimated should be selected. The gain calculation, the parameter update, and the covariance matrix update of RLS are identical to those of KF [24], [25]. In order to estimate the parameters, K_ϕ, C_ϕ,

I_{xx} and h_s, the matrices in (5) should be set as given in (18).

$$\begin{cases} \mathbf{x}_p(k+1) = \mathbf{x}_p(k) + \boldsymbol{\mu}_2(k) \\ \mathbf{y}(k) = \phi^T(k)\,\mathbf{x}_p(k) + \boldsymbol{\eta}_2(k) \end{cases} \tag{13}$$

$$\mathbf{M}_2(k) = \mathbb{E}\left\{\boldsymbol{\mu}_2(k)\,\boldsymbol{\mu}_2^T(k)\right\},\ \mathbf{N}_2(k) = \mathbb{E}\left\{\boldsymbol{\eta}_2(k)\,\boldsymbol{\eta}_2^T(k)\right\}$$

$$\begin{cases} \mathbf{x}_p(k) = \left[\, K_\phi \;\; C_\phi \,\right]^T, \quad \phi^T(k) = \left[\, \hat{\phi}(k) \;\; \hat{\dot{\phi}}(k) \,\right] \\ y(k) = -I_{xx}\ddot{\phi}(k) + M_\phi(k) + m_s h_s a_y(k) \end{cases} \tag{14}$$

$$\begin{cases} \mathbf{x}_p(k) = \left[\, K_\phi \;\; C_\phi \;\; I_{xx} \,\right]^T, \\ \qquad \phi^T(k) = \left[\, \hat{\phi}(k) \;\; \hat{\dot{\phi}}(k) \;\; \hat{\ddot{\phi}}(k) \,\right] \\ y(k) = M_\phi(k) + m_s h_s a_y(k) \end{cases} \tag{15}$$

$$\begin{cases} \mathbf{x}_p(k) = \left[\, K_\phi \;\; C_\phi \;\; h_s \,\right]^T, \\ \qquad \phi^T(k) = \left[\, \hat{\phi}(k) \;\; \hat{\dot{\phi}}(k) \;\; m_s a_y(k) \,\right] \\ y(k) = -I_{xx}\ddot{\phi}(k) + M_\phi(k) \end{cases} \tag{16}$$

$$\begin{cases} \mathbf{x}_p(k) = \left[\, K_\phi \;\; C_\phi \;\; I_{xx} \;\; h_s \,\right]^T \\ \phi^T(k) = \left[\, \hat{\phi}(k) \;\; \hat{\dot{\phi}}(k) \;\; \hat{\ddot{\phi}}(k) \;\; m_s a_y(k) \,\right] \\ y(k) = M_\phi(k) \end{cases} \tag{17}$$

$$\mathbf{F} = \mathbf{I},\quad \mathbf{G} = \mathbf{0},\quad \mathbf{H} = \mathbf{0},\quad \mathbf{C} = \phi^T(k),$$
$$\mathbf{M} = \mathbf{M}_2,\quad \mathbf{N} = \mathbf{N}_2 \tag{18}$$

D. DUAL KALMAN FILTER FOR STATE AND PARAMETER ESTIMATION

By combining two Kalman filters, as given in (9) and (18), the state, i.e., the roll angle, and the parameters are estimated simultaneously. This is called a dual KF [24], [25]. Fig. 2 shows the overall structure of observer-based active roll controller with a dual KF. Fig. 4 shows the block diagram of the dual KF, which enlarges the dual KF in Fig. 2. In Fig. 4, $\hat{\mathbf{x}}_s$ is the vector of estimated states as given in (8), and $\hat{\mathbf{x}}_p$ is the vector of estimated parameters as given in (14). As shown in Fig. 4, the output of the time update of the state estimator is fed into the measurement update of the parameter estimator, and the output of the time update of the parameter estimator is fed into that of state estimator. By virtue of the parameter estimator, the dual KF can be robust against parameter uncertainties.

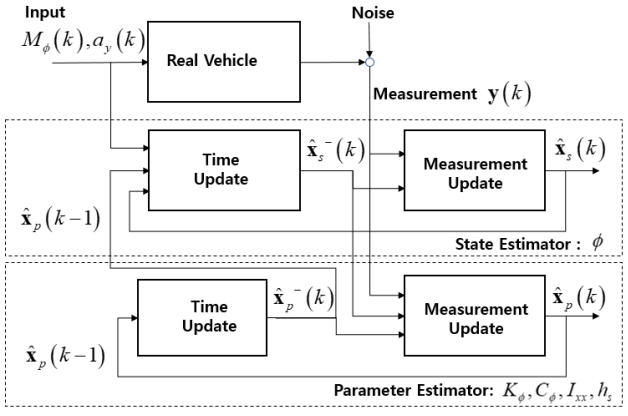

FIGURE 4. Dual Kalman filter for state and parameter estimation in ARC.

The values of parameters in the parameter estimators from (14) to (17) are bounded between upper and lower limits. For example, the parameters in (17) are always positive. With these limits and (10), the observer-based control system with LQR, H_∞, sliding mode controllers and dual KF is guaranteed to be globally stable.

E. KALMAN FILTER WITH CONSTANT VELOCITY MODEL

In this paper, Kalman filter with constant velocity model (KFCVM) is adopted as a state observer. Eq. (19) shows the simple kinematic relationship between the roll angle and the roll rate obtained by neglecting the pitch and yaw motions. With the state vector definition (20), the constant velocity model for roll motion is given as (21) with the state-space form in the continuous-time domain. As shown in (21), the sensor output is the roll rate. In (21), $\mu_3(k)$ and $\eta_3(k)$ are the vectors of the system and measurement noise processes, respectively. The discrete-time state-space equation (22) is obtained by discretizing (21) with the sampling time of T_s. The covariance matrices of the system and measurement noise processes are given in (23). For state estimation, the matrices in (5) should be set as given in (24) from the discrete-time state-space equation (22). As given in (23), the tuning parameters of KFCVM are the variances σ_q^2 and σ_r^2 of the system and measurement noise processes, respectively.

As shown in the output equation of (22), the measurement is the roll rate. So, the roll angle can be estimated with the KF (24) from the roll rate measurement. In case of this, KFCVM is a simple integration method used to estimate the roll angle from roll rate measurement. If the output matrix in (22) is set as $\mathbf{C} = [1\ 0]$ and the sensor output is the roll rate, then the roll angular acceleration can be obtained from KFCVM. In case of this, KFCVM is a simple differentiation method used to estimate the roll angular acceleration from roll rate measurement. When using (15) and (17), the roll angular acceleration is estimated by KFCVM with roll rate measurement. This is the idea of the previous work [28]. By virtue of the simple integration on the roll rate signal, the KFCVM is independent of the parameters of the roll model (3). So, KFCVM is expected to be robust against parameter uncertainties.

KFCVM has two functions: state estimation and noise filtering [26], [27]. In the previous work, KFCVM was used as a noise filter [4]. In this paper, KFCVM is used for noise filtering on measured roll rate and lateral acceleration.

$$\phi(t) = \int_0^t \dot{\phi}(t) \Leftrightarrow \dot{\phi}(t) = \frac{d\phi(t)}{dt} \tag{19}$$

$$\mathbf{x}_v(t) = \left[\, \phi(t) \quad \dot{\phi}(t) \,\right]^T \tag{20}$$

$$\begin{cases} \dot{\mathbf{x}}_v(t) = \begin{bmatrix} 0 & 1 \\ 0 & 0 \end{bmatrix} \mathbf{x}_v(t) + \boldsymbol{\mu}_3(t) \\ \mathbf{y}(t) = \begin{bmatrix} 0 & 1 \end{bmatrix} \mathbf{x}_v(t) + \boldsymbol{\eta}_3(t) \end{cases} \tag{21}$$

$$\begin{cases} \mathbf{x}_v(k+1) = \begin{bmatrix} 1 & T_s \\ 0 & 1 \end{bmatrix} \mathbf{x}_v(k) + \boldsymbol{\mu}_3(k) \\ \mathbf{y}(k) = \begin{bmatrix} 0 & 1 \end{bmatrix} \mathbf{x}_v(k) + \boldsymbol{\eta}_3(k) \end{cases} \tag{22}$$

$$\begin{cases} \mathbf{M}_3(k) = \mathbb{E}\left\{\boldsymbol{\mu}_3(k)\,\boldsymbol{\mu}_3^T(k)\right\} = \sigma_q^2 \begin{bmatrix} T_s^3/3 & T_s^2/2 \\ T_s^2/2 & T_s \end{bmatrix} \\ \mathbf{N}_3(k) = \mathbb{E}\left\{\boldsymbol{\eta}_3(k)\,\boldsymbol{\eta}_3^T(k)\right\} = \sigma_r^2 \end{cases} \quad (23)$$

$$\mathbf{F} = \begin{bmatrix} 1 & T_s \\ 0 & 1 \end{bmatrix}, \quad \mathbf{G} = \mathbf{0}, \quad \mathbf{H} = \mathbf{0}, \quad \mathbf{C} = \begin{bmatrix} 0 & 1 \end{bmatrix},$$
$$\mathbf{M} = \mathbf{M}_3, \quad \mathbf{N} = \mathbf{N}_3 \quad (24)$$

IV. SIMULATION AND EXPERIMENT

In this section, the observer-based active roll control system with three controllers and the designed KFs is validated through simulation on the vehicle simulation software, CarSim, and experiment on a test vehicle. The structure of the observer-based active roll control system is given in Fig. 2.

A. SIMULATION ON CARSIM

In this subsection, the estimation performance of KFs under parameter uncertainties is evaluated through simulation conducted on CarSim. As given in the Section II, LQR, H_∞ control and SMC have been designed in the observer-based active roll control system. The weights in LQ objective function and the sliding surface were set as given in the previous work [3]. The covariance matrices of system and measurement noises for KFs are given in Table 1. The sampling times of the measurement and the controllers were set to 10ms. The observer-based active roll control system was implemented on MATLAB/Simulink.

TABLE 1. Variances of system and measurement noises.

M(k)	$\begin{bmatrix} 1e-4 & 0 \\ 0 & 1e+4 \end{bmatrix}$	N(k)	1e–4
$M_2(k)$	$\begin{bmatrix} 1e-1 & 0 \\ 0 & 1e-1 \end{bmatrix}$	$N_2(k)$	1.00
σ_q	1e2	σ_r	1e-2

The driving scenario for simulation was a closed-loop steering on the moose test track with the driver model given in CarSim [3], [4], [10]. Fig. 5 shows the moose test track used for simulation [30]. The initial vehicle speed was set to be 80km/h, and the tire-road friction was set to be 0.6. For generation of control roll moment, AARB was adopted as an actuator. AARB was modeled as the first-order system with the time constant of 0.05. For a lateral stability under ARC, the unified chassis control with ESC and AFS has keep activated [30]. The AARB was implemented to be an actuator for ARC.

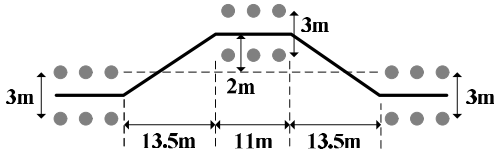

FIGURE 5. Moose test track representing double lane change maneuver.

The parameters to be estimated are the roll stiffness and the roll damping, as shown in (14). To validate the estimation performance of the designed KFs, the sets of parameters of the 1-DOF roll model were randomly generated from the following ranges: $200 \le I_{xx} \le 2,000$, $700 \le m_s \le 2,000$, $0.2 \le h_s \le 1.2$, $1,000 \le C_\phi \le 20,000$, $2,000 \le K_\phi \le 150,000$. For a realistic simulation, a band-limited white noise was added to the roll rate signal from CarSim. This reflects the fact that the measured roll rate signal from cheap sensors are noisy. The noisy roll rate signals can generate the fluctuation in the control roll moment although it is filtered from KFs. The KFCVM was applied to the roll rate signal for noise filtering and to obtain the roll angular acceleration.

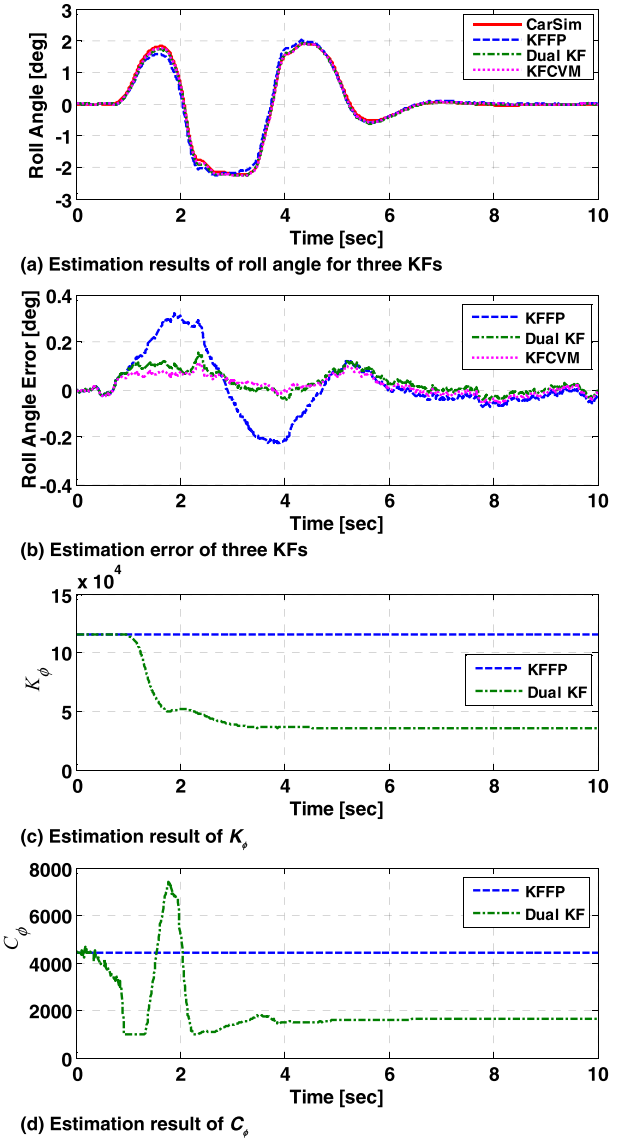

FIGURE 6. State and parameter estimation results without filtering on the roll rate for each KF.

Figs. 6 and 7 show the estimation results of three KFs without and with filtering on the roll rate, respectively. These results were obtained with a single set of randomly generated

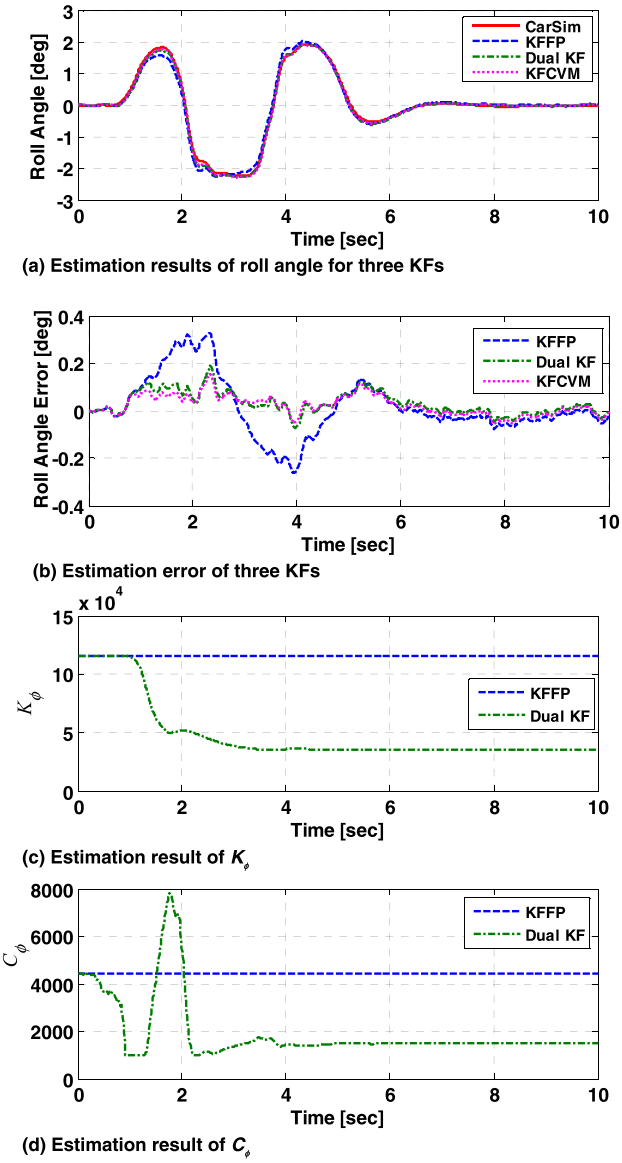

FIGURE 7. State estimation results with filtering on the roll rate for each KF.

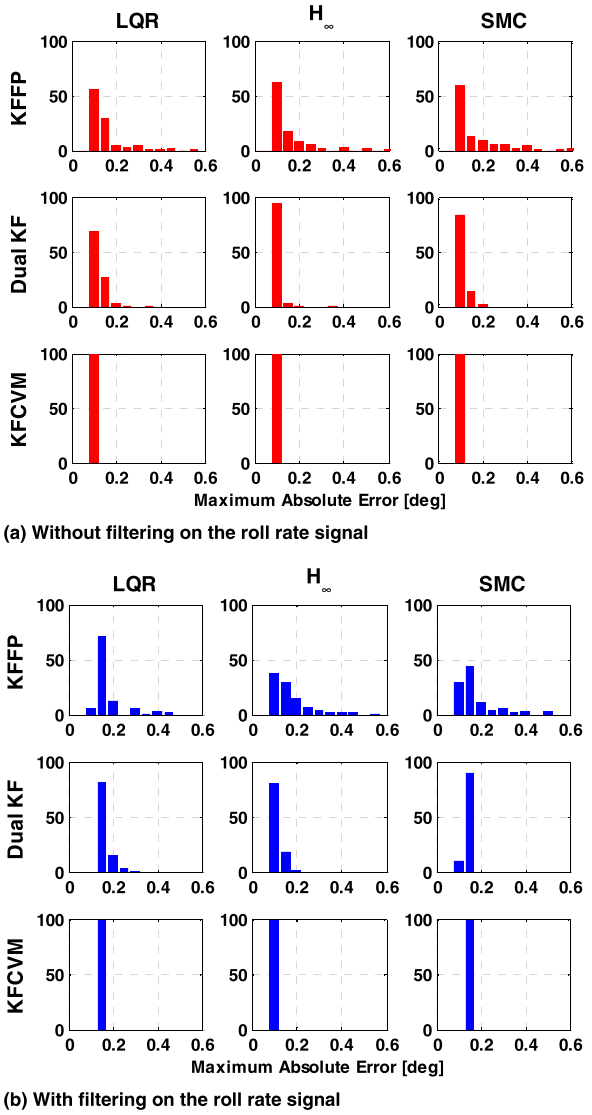

FIGURE 8. Estimation results for three KFs and three active roll controllers in terms of the maximum absolute error.

parameters, selected among 100 sets. In order to obtain the simulation results, LQR was used as an active roll controller, and the dual KF was used as state and parameter estimators. In Figs. 6 and 7, the legend KFFP represents the Kalman filter with fixed parameters. As shown in Figs. 6 and 7, the dual KF and KFCVM have almost identical performance in estimating the roll angle. However, KFFP shows worse performance compared to the dual KF and KFCVM. This is due to the fact that the differences between the fixed and estimated parameters of KFFP and dual KF are large, as shown in Fig. 6-(c), -(d), Fig. 7-(c) and -(d). In Fig. 6-(c) and -(d), the differences between the fixed and estimated values of the roll stiffness and the roll damping are about 80,000 and 3,000, respectively.

To investigate the robustness of three KFs, simulation was conducted with 100 sets of randomly generated parameters of 1-DOF roll model. The estimated parameters in the model are the roll stiffness and the roll damping, as given in (14). Figs. 8 and 9 shows the histograms of the maximum absolute and the root mean square(RMS) values of the roll angle errors in the case of with and without filtering on the roll rate for three active roll controllers and three KFs, respectively. As shown in Figs. 8 and 9, the dual KF is more robust than KFFP for all active roll controllers regardless of the noise filtering on the roll rate. As expected, KFCVM is the most robust observer among KFs because it is independent of the model parameters, i.e., the roll stiffness and the roll damping.

Figs. 8 and 9 show the effects of noise filtering of KFCVM. In the case of KFFP, the noise filtering on the roll rate gave larger variance than no filtering case in terms of the maximum absolute errors. This is caused by the time delay in filtering with KFCVM. The maximum absolute errors of dual KF and KFCVM were also increased due to the time delay. H_∞ control and SMC show larger variance than LQR because the high gain of them amplifies roll angle errors.

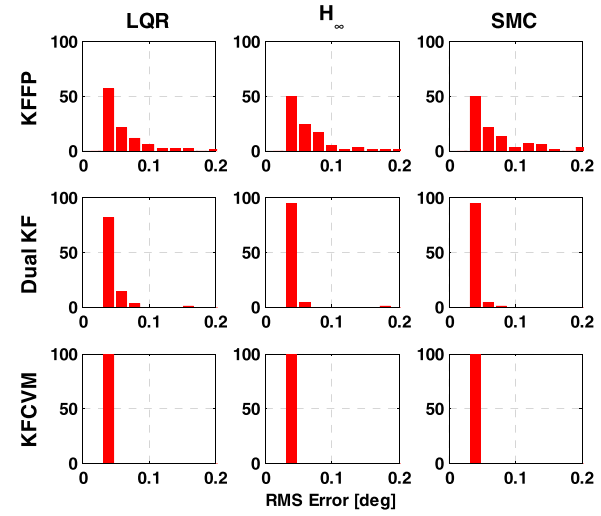

(a) Without filtering on the roll rate signal

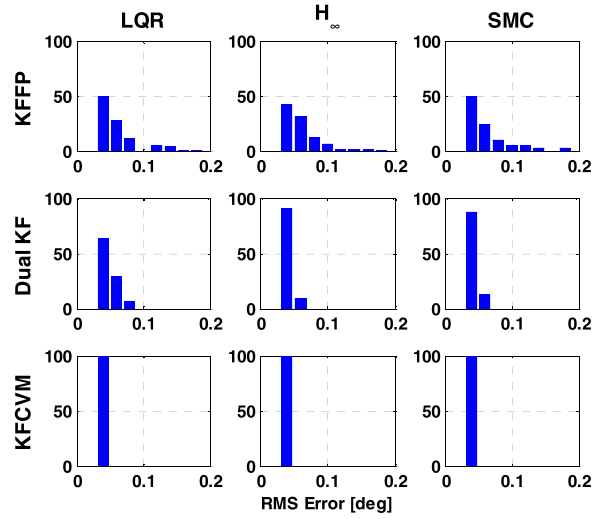

(b) With filtering on the roll rate signal

FIGURE 9. Estimation results for three KFs and three active roll controllers in terms of RMS error.

On the other hand, the noise filtering has slight effect on the estimation performance for dual KF and KFCVM due to the parameter estimation of dual KF and the parameter independency of KFCVM. Moreover, the filtering on the roll rate has little effect on the estimation performance of three KFs in terms of the RMS errors.

B. EXPERIMENT ON A REAL VEHICLE

In real experiments, it is hard for one to implement an actuator for ARC because it costs a lot of money and is time-consuming [8]. So, the estimation performance and robustness of the designed KFs, i.e., KFFP, dual KF and KFCVM, without active roll controllers is checked with experiment in this subsection.

Experiment scenario was a double lane change by a real driver. The vehicle used for experiment was a small-sized SUV, as shown in Fig. 10. The speed of the vehicle in experiment was set to be 60km/h and maintained to be constant. For comparison, the accurate roll angle is measured by

FIGURE 10. The small-sized SUV used for experiment.

RT 3000 and its base station of Oxford Technical Solutions Ltd [31]. The accuracy of roll and pitch angles measured by RT3000 is 0.05° 1σ. The roll rate and lateral acceleration used for KFs were measured with HG1120 of Honeywell AeroSpace [13]. Three KFs were implemented with MATLAB/Simulink and run on dSpace MicroAutoBox. So, the data from the sensors and the output of KFs were saved using dSpace MicroAutoBox [32]. To check the estimation performance and the robustness of three KFs, the outputs of KFs, i.e., the estimated roll angles, are compared to the accurate one obtained from RT3000.

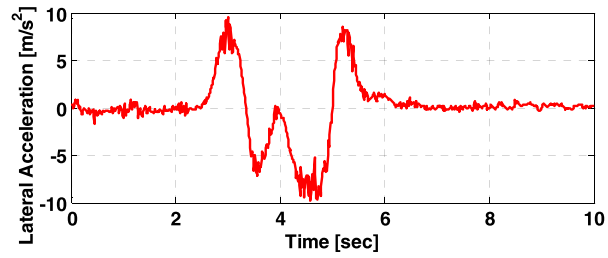

(a) Measured lateral acceleration

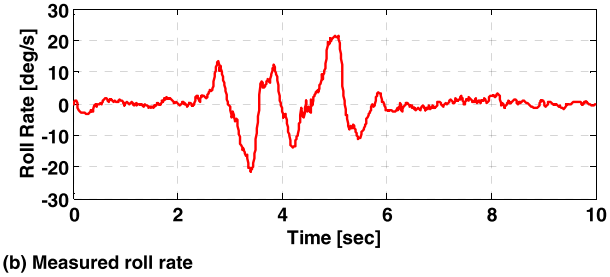

(b) Measured roll rate

FIGURE 11. Measured signals with HG1120 from experiment.

Fig. 11 shows the lateral acceleration and roll rate measured with HG1120 from experiment. As shown in Fig. 11, the measured lateral acceleration is noisy, compared to the roll rate. The measured roll rate is also noisy. So, it is necessary to apply KFCVM as a filter in order to reduce the fluctuations in the control roll moment. Fig. 12 shows the estimation results of three KFs obtained from experiment. In Fig. 12, the legend Real means the accurate roll angle measured with RT3000. Similar to the simulation results, the dual KF and KFCVM have nearly identical performance

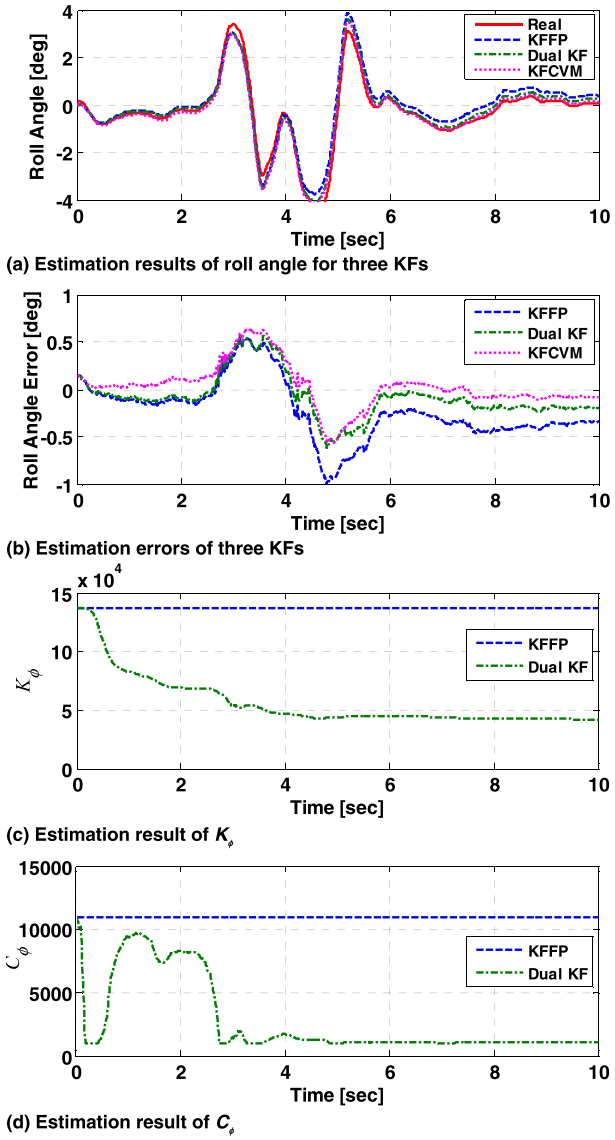

FIGURE 12. Estimation results of three KFs from experiment.

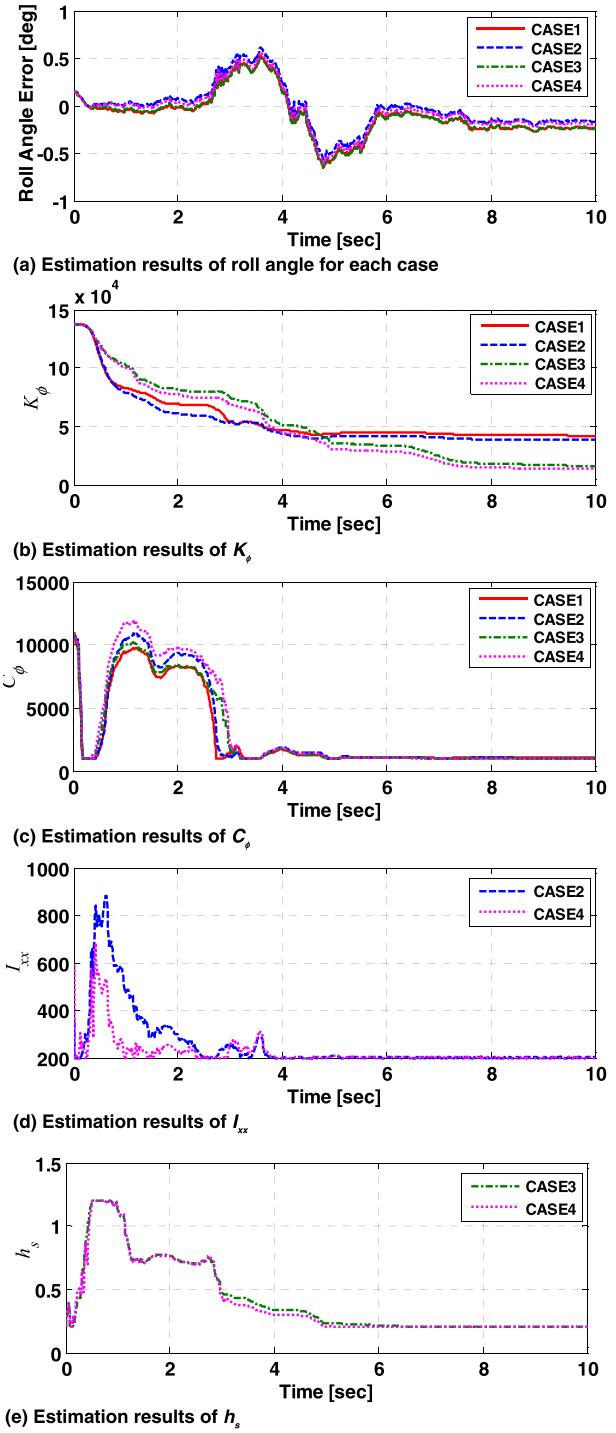

FIGURE 13. Estimation results of dual KF for each case.

in estimating the roll angle. On the other hand, KFFP shows worse performance compared to dual KF and KFCVM in terms of the roll angle error. As shown in Fig. 11-(c) and -(d), the differences between the fixed and estimated values of the roll stiffness and the roll damping are quite large. As a result, it caused the difference of roll angle error between KFFP and dual KF. Moreover, the estimated values of the roll stiffness and the roll damping are similar to those of simulation. In other words, as shown in Fig. 6-(c), -(d), Fig. 7-(c), -(d), Fig. 12-(c), and -(d), the estimated values of the roll stiffness and the roll damping converged to nearly identical ones, respectively.

To evaluate the parameter estimation performance of dual KF for the parameter sets, (14), (15), (16) and (17), simulation was conducted with the experimental data, i.e., the measured lateral acceleration and roll rate from HG1120 as shown in Fig. 11. Let CASE1, CASE2, CASE3 and CASE4 denote the sets of parameters in (14), (15), (16) and (17), respectively. For each case, the estimated roll angles of three KFs are compared with accurate one measured with RT3000.

Fig. 13 shows the estimation results of dual KF for each set of parameters. As shown in Fig. 13-(a), there are small differences in roll angle error for each case. In other words, it is enough for on to use the dual KF with the parameter set, (14), for state and parameter estimation. This means that adaptation mechanism of the parameter estimator or dual KF for the roll stiffness and the roll damping, (14), can reflect the

uncertainties or variations in the roll moment of inertia and the height of center of gravity. It is notable that the estimated values of the roll damping, the roll moment of inertia and the height of center of gravity converged to the corresponding lower limits except the roll stiffness. This means that the roll stiffness is the most important among the model parameters in terms of parameter estimation, and that it is desirable to set the initial values of the parameters as small as possible.

To check the robustness of three KFs, simulation was conducted with experimental data, i.e., the measured lateral acceleration and roll rate from HG1120 as shown in Fig. 11. Three KFs were run with 300 sets of randomly generated parameters of the 1-DOF roll model. The ranges of the parameters are identical to those in the previous subsection. The roll stiffness and the roll damping, as given in (14), were selected for parameter estimation. KFCMV was used to filter the measured roll rate and lateral acceleration.

Fig. 14 shows the histograms of the maximum absolute and RMS values of the estimation errors obtained from three KFs

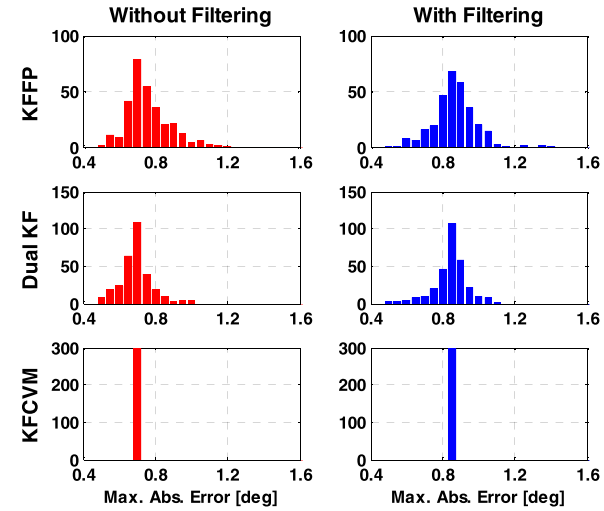

(a) Maximum absolute error performance

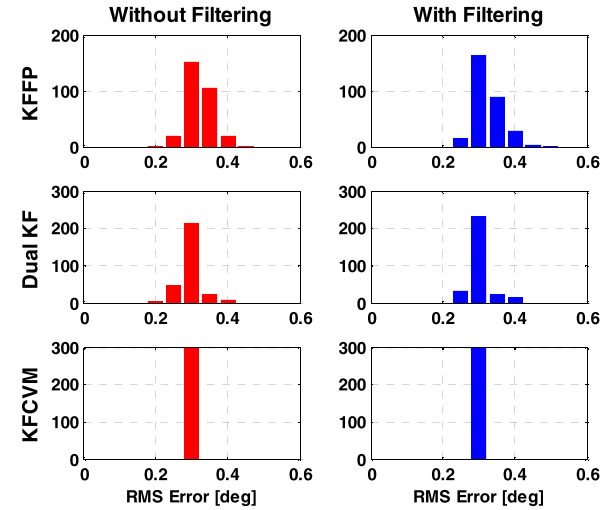

(b) Root mean square error performance

FIGURE 14. Estimation results of three KFs from experiment.

and experimental data. As shown in Fig. 14, the dual KF is more robust compared to KFFP in terms of the maximum absolute and RMS estimation errors. In other words, the variance of estimation errors of KFFP is larger than that of the dual KF. However, the estimation performance of dual KF in terms of the maximum absolute error is not as notable as the simulation results of the previous subsection. In other words, the maximum absolute errors of dual KF in Fig. 14-(a) was not notably improved, compared to Fig. 8-(a) and Fig. 9-(a). On the other hand, the RMS values of estimation error of Dual KF got better than those of KFFP, as shown in Fig. 14-(b). As expected, KFCVM is the most robust observer among three KFs.

As shown in Fig. 14-(a), the noise filtering on the roll rate and the lateral acceleration deteriorates the estimation performance of three KFs in terms of the maximum absolute error. This is caused by the time delay from the filter, i.e., KFCVM. On the other hand, the noise filtering has little effect on the RMS errors, as shown in Fig. 14-(b). This is identical to the simulation results of the previous subsection.

V. CONCLUSION

In this paper, the observer-based active roll control system was designed. The dual KF and KFCVM were adopted as a robust observer in order to cope with the parameter uncertainty and nonlinearity in the vehicle model. Notable feature of the dual KF is that it has parameter estimation function against the parameter variation and the nonlinearity. KFCVM was expected to be robust against the parameter uncertainty because it is independent of model parameters. The KF with fixed parameter was used for comparison. To check the performance of observer-based active roll control system, three active roll controllers – LQR, H_∞ and sliding mode controller – and three KFs were designed. The estimation performance and robustness of three KFs were checked through simulation on CarSim and vehicle tests. From the simulation and experiment, it had been shown from both simulations and vehicle tests that the dual KF is more robust than KF with fixed parameters. As expected, KFCVM is quite robust due to the parameter independency of model parameters. Another conclusion is that it is desirable for one to set initial values of parameters for KFs be set as small as possible for good estimation performance.

REFERENCES

[1] A. Sorniotti, A. Morgando, and M. Velardocchia, "Active roll control: System design and hardware-in-the-loop test bench," *Vehicle Syst. Dyn.*, vol. 44, no. 1, pp. 489–505, 2006.
[2] Y. Mizuta, M. Suzumura, and S. Matsumoto, "Ride comfort enhancement and energy efficiency using electric active stabiliser system," *Vehicle Syst. Dyn.*, vol. 48, no. 11, pp. 1305–1323, 2010.
[3] S. Yim, "Design of preview controllers for active roll stabilization," *J. Mech. Sci. Technol.*, vol. 32, no. 4, pp. 1805–1813, 2018.
[4] J. Nah and S. Yim, "Observer-based active roll preview control with V2V communication," *IEEE Access*, vol. 7, pp. 44831–44839, 2019.
[5] R. C. Lin, D. Cebon, and D. J. Cole, "Active roll control of articulated vehicles," *Vehicle Syst. Dyn.*, vol. 26, no. 1, pp. 17–43, 1996.
[6] D. J. M. Sampson and D. Cebon, "Active roll control of single unit heavy road vehicles," *Vehicle Syst. Dyn.*, vol. 40, no. 4, pp. 229–270, 2003.

[7] H. J. Kim and Y. P. Park, "Investigation of robust roll motion control considering varying speed and actuator dynamics," *Mechatronics*, vol. 14, pp. 35–54, Feb. 2004.
[8] K. Jeon, H. Hwang, S. Choi, J. Kim, K. Jang, and K. Yi, "Development of an electric active rollcontrol (ARC) algorithm for a SUV," *Int. J. Automot. Technol.*, vol. 13, no. 2, pp. 247–253, 2012.
[9] Y. Ohta, H. Kato, D. Yamada, K. Sato, T. Fukino, E. Nobuyama, and S. Buma, "Development of an electric active stabilizer system based on robust design," SAE Tech. Paper 2006-01-0758, 2006.
[10] S. Yim and K. Yi, "Design of an active roll control system for hybrid four-wheel-drive vehicles," *Proc. Inst. Mech. Eng., D, J. Automobile Eng.*, vol. 227, no. 2, pp. 151–163, 2013.
[11] J. G. Guzman, L. P. Gonzalez, J. P. Redondo, S. S. Sanchez, and B. L. Boada, "Design of low-cost vehicle roll angle estimator based on Kalman filters and an IoT architecture," *Sensors*, vol. 18, no. 6, p. 1800, 2018.
[12] *VBOX Automotive, VBOX 3i, 100 Hz Data Logger*. Accessed: 2019. [Online]. Available: https://www.vboxautomotive.co.uk/index.php/ko/products/data-loggers/vbox-3i
[13] Honeywell Aerospace. *HG1120 MEMS Inertial Measurement Unit*. Accessed: 2018. [Online]. Available: https://aerospace.honeywell.com/en/~/media/aerospace/files/brochures/n61-1524-000-004-hg1120-mems-inertial-measurement-unit-bro.pdf
[14] W. Kerstens, "Robust observer roll rate sensor fault detection," SAE Tech. Paper 2017-01-1572, 2017.
[15] B. L. Boada, M. J. L. Boada, L. Vargas-Melendez, and V. Diaz, "A robust observer based on H filtering with parameter uncertainties combined with neural networks for estimation of vehicle roll angle," *Mech. Syst. Signal Process.*, vol. 99, pp. 611–623, Jan. 2018.
[16] M. Jalali, E. Hashemi, A. Khajepour, S.-K. Chen, and B. Litkouhi, "Model predictive control of vehicle roll-over with experimental verification," *Control Eng. Pract.*, vol. 77, pp. 95–108, Aug. 2018.
[17] H. Dahmani, O. Pagès, A. El Hajjaji, and N. Daraoui, "Observer-based robust control of vehicle dynamics for rollover mitigation in critical situations," *IEEE Trans. Intell. Transp. Syst.*, vol. 15, no. 3, pp. 274–284, Sep. 2014.
[18] A.-T. Nguyen, C. Sentouh, and J.-C. Popieul, "Fuzzy steering control for autonomous vehicles under actuator saturation: Design and experiments," *J. Franklin Inst.*, vol. 355, no. 18, pp. 9374–9395, Dec. 2018.
[19] Z. Wang, Y. Qin, C. Hu, M. Dong, and F. Li, "Fuzzy observer-based prescribed performance control of vehicle roll behavior via controllable damper," *IEEE Access*, vol. 7, pp. 19471–19487, 2019.
[20] R. Rajamani, D. Piyabongkarn, V. Tsourapas, and J. Y. Lew, "Parameter and state estimation in vehicle roll dynamics," *IEEE Trans. Intell. Transp. Syst.*, vol. 12, no. 4, pp. 1558–1567, Sep. 2011.
[21] R. Tafner, M. Reichhartinger, and M. Horn, "Robust vehicle roll dynamics identification based on roll rate measurements," *IFAC Proc. Volumes*, vol. 45, no. 30, pp. 72–78, 2012.
[22] K. Nam, S. Oh, H. Fujimoto, and Y. Hori, "Estimation of sideslip and roll angles of electric vehicles using lateral tire force sensors through RLS and Kalman filter approaches," *IEEE Trans. Ind. Electron.*, vol. 60, no. 3, pp. 988–1000, Mar. 2013.
[23] K. Jiang, A. C. Victorino, and A. Charara, "Adaptive estimation of vehicle dynamics through RLS and Kalman filter approaches," in *Proc. 18th IEEE Int. Conf. Intell. Transp. Syst.*, Canary Islands, Spain, Sep. 2015, pp. 1741–1746.
[24] T. A. Wenzel, K. J. Burnham, M. V. Blundell, and R. A. Williams, "Dual extended Kalman filter for vehicle state and parameter estimation," *Vehicle Syst. Dyn.*, vol. 44, no. 2, pp. 153–171, 2006.
[25] D. Hu, C. Zong, and X. Na, "Combined estimation of vehicle states and road friction coefficients using dual extended Kalman filter," in *Proc. AVEC*, 2010, pp. 309–314.
[26] L. Hong, "Discrete constant-velocity-equivalent multirate models for target tracking," *Math. Comput. Model.*, vol. 28, no. 11, pp. 7–18, 1998.
[27] X. Tian, G. Chen, E. Blasch, K. Pham, and Y. Bar-shalom, "Comparison of three approximate kinematic models for space object tracking," in *Proc. Int. Conf. Inf. Fusion*, Jul. 2013, pp. 1005–1012.
[28] A. Hac, D. Nichols, and D. Sygnarowicz, "Estimation of vehicle roll angle and side slip for crash sensing," SAE Tech. Paper 2010-01-0529, 2010.
[29] D. Simon, *Optimal State Estimation: Kalman, H Infinity, and Nonlinear Approaches*. Hoboken, NJ, USA: Wiley, 2006.
[30] S. Yim, "Unified chassis control with electronic stability control and active front steering for under-steer prevention," *Int. J. Automot. Technol.*, vol. 16, no. 5, pp. 775–782, 2015.
[31] Oxford Technical Solutions. *RT3000, High performance GNSS/INS for Dynamic Applications*. Accessed: 2019. [Online]. Available: https://www.oxts.com/products/rt3000/
[32] dSpace. *MicroAutoBox II*. Accessed: 2019. [Online]. Available: https://www.dspace.com/en/inc/home/medien/product_info/prodinf_mabx.cfm

MANBOK PARK received the B.S. degree in mechanical engineering from Inha university, South Korea, the M.S. degree in mechanical engineering from the Korea Advanced Institute of Science and Technology (KAIST), South Korea, in 2002, and the Ph.D. degree from the Graduate School of Convergence Science and Technology, Seoul National University, South Korea, in 2014.

He had been worked for 15 years with Mando Corporation, automotive part company. He is currently an Assistant Professor of electrical engineering with the Korea National University of Transportation. His research interests are autonomous vehicle, SLAM, precision map, risk assessment, and artificial intelligence.

SEONGJIN YIM received the B.S. degree in mechanical engineering from Yonsei University, South Korea, in 1995, and the M.S. and Ph.D. degrees in mechanical engineering from the Korea Advanced Institute of Science and Technology (KAIST), in 1997 and 2007, respectively.

From 2008 to 2010, he was a Postdoctoral Researcher with BK21 School for Creative Engineering Design of Next Generation Mechanical and Aerospace Systems, Seoul National University. From 2011 to 2013, he was a Research Professor with the Advanced Institutes of Convergence Technology, Seoul National University. Since 2013, he has been an Assistant Professor with the Department of Mechanical and Automotive Engineering, Seoul National University of Science and Technology, South Korea. His research interests include integrated chassis control systems with V2V communication, cloud computing-based vehicle control, electric power steering, and steer-by-wire systems.